International Journal of Environmental Science and Technology
https://doi.org/10.1007/s13762-020-02873-z

ORIGINAL PAPER

Biovalorization of mandarin waste peels into silver nanoparticles and activated carbon

B. A. Omran[1] · O. Aboelazayem[2] · H. N. Nassar[1,3,4] · R. A. El-Salamony[1] · N. Sh. El-Gendy[1,4,5]

Received: 19 April 2020 / Revised: 7 June 2020 / Accepted: 27 July 2020
© Islamic Azad University (IAU) 2020

Abstract

This work aims to upcycle mandarin (*Citrus reticulum*) waste peels into valuable compounds with different applications. The one-factor-at-a-time method was applied to optimize the biosynthesis of silver nanoparticles using the hot water extract of mandarin peels' waste. The maximum production reached 2.5 g L^{-1} in a 4-h, pH9, 100 rpm continuous stirring batch process, operating at 30 °C, under fluorescent illumination of 36 W/6400 K, using 3000 mg L^{-1} extract solution and 2 mmol $AgNO_3$. Dynamic light scattering, zeta potential, X-ray diffraction, energy-dispersive X-ray, Fourier transform infrared spectroscopy, field emission scanning electron microscope and high-resolution transmission electron microscope were employed to characterize the prepared silver nanoparticles, which revealed highly stable, uniformly distributed, nonagglomerated crystalline silver nanoparticles, with spherical/oval shapes and a size range of 10–19 nm. The preliminary cost analysis proved the cost-effectiveness of the valorization of mandarine peels into silver nanoparticles, which costs approximately 7.6 US$/g green synthesized silver nanoparticles with good savings relative to the global prices of the chemically synthesized ones. Moreover, to reach the point of zero waste and maximize the profitability of the valorization, the mandarin spent waste disposed from the batch process were upcycled to activated carbon which has different applications.

Keywords Cost analysis · Green synthesis · Nanomaterials · Spectroscopic and microscopic characterization · Solid waste management · Zero waste

Introduction

Solid waste management (SWM) is a worldwide critical mandate (Fulekar et al. 2018). Open burning of agricultural wastes is assumed to be one of the main causes of air pollution and climate change (Santiago-De la Rosa et al. 2018). Moreover, citrus fruit wastes are one of the main municipal solid wastes (MSW). Currently, landfilling and incineration are the two main techniques that are usually employed to get rid of such MSW. This consequently has many adverse effects on human health, ecosystems, tourism, coastal development, biodiversity and availability of water resources, food and agricultural security (Apergis et al. 2020; Kenawy et al. 2020).

Several publications illustrated that versatile biologically originated compounds exist in these wastes which can be extensively employed to produce high-value chemicals, bioactive compounds, pharmaceuticals, biofuels, biocides, corrosion inhibitors and medicinal products (Galanakis 2012; Ravindran and Jaiswal 2016; Ghosh et al. 2017; El-Gendy et al. 2018; Kheiralla et al. 2018). Besides, current

Professor Nour Sh. El-Gendy is affiliated to Head Manager of Petroleum Biotechnology Lab., Egyptian Petroleum Research Institute (EPRI)

Editorial responsibility: Samareh Mirkia.

✉ N. Sh. El-Gendy
nourepri@yahoo.com

1 Department of Process Design and Development, Egyptian Petroleum Research Institute (EPRI), Nasr City, Cairo PO 11727, Egypt

2 Department of Chemical and Environmental Engineering, Faculty of Engineering, University of Nottingham, Nottingham NG7 2RD, UK

3 Department of Microbiology, Faculty of Pharmacy, October University for Modern Sciences and Arts (MSA), 6th of October City PO 12566, Egypt

4 Nanobiotechnology Program, Faculty of Nanotechnology for Postgraduate Studies, Cairo University, Sheikh Zayed Branch Campus, Sheikh Zayed City, Giza PO 12588, Egypt

5 Center of Excellence, October University for Modern Sciences and Arts (MSA), 6th of October City, Giza, PO 12566, Egypt

investigations proved the capability to valorize such wastes into high-valued nanoparticles (Shah et al. 2015; Ali et al. 2017; Omran et al., 2018a). Many valuable biomolecules and constituents exist in these wastes and have the capability to act as efficient, sustainable and eco-friendly reductants to the precursor metal ions. Not only this, but they act also as modeling, capping and stabilizing agents, to avoid the agglomeration of the prepared nanoparticles (Ali et al. 2017; Nava et al. 2017; Omran et al., 2018a).

According to the United States Department of Agriculture (USDA) in 2017, the global production of mandarin/tangerine for 2016/2017 is forecasted at 28.4 million metric tons (USDA 2017). In Egypt, balady mandarin (*Citrus reticulum*) is the second citrus fruit after balady orange (Mohamed 2015). Citrus fruits are usually consumed either as processed juices or fresh as they are. They are widely used in food, cosmetics and pharmaceutical industries owing to their characteristic odor and flavor (Czech et al. 2020). Thus, because of the high production, consumption and the industrial use of citrus fruits, their wastes are expected to be generated in large quantities. The main solid wastes of citrus food processing are peels, seeds and rags (membranes and cores) (Milik 2011). The citrus waste constitutes approximately 50–70% of the fruit, of which about 60–65% is peel. Nevertheless, 7–16% of the total mandarin fruit weight is reported to be waste peels, which represents 25–30% of the total mandarin fruit solid waste (Mamma and Christakopoulos 2008; Sagar et al. 2018; Mahato et al. 2019). Consequently, very large amounts of peels were estimated to be worldwide annually produced.

Recently, an extensive focus was directed toward the green fabrication of nanoparticles (NPs) which gained considerable significant interest, as being an environmentally benign and cost-effective process (Ahmad et al. 2016). It can be carried out via bacteria (Vairavel et al. 2020), fungi (Omran et al. 2018b, 2019), yeast (Sriramulu and Sumathi 2018), algae (Arya et al. 2019), plant extracts (Thatikayala et al. 2019) and agro-industrial wastes (Ali et al. 2017; Omran et al. 2018a, b; Sinsinwar et al. 2018; Zamani et al. 2019; Narasaiah and Mandal 2020).

It is taken into consideration that the readily abundant mandarin peels are available at zero cost. Also, they are rich in required bioactive compounds for green synthesis of nanoparticles, including phenolic acids, saturated fatty acids and sugar-derivative compounds (Omran et al. 2013). Henceforth, this study aimed to focus on waste minimization and upcycling of the mandarin peels' wastes as a green synthesizer for AgNPs under mild operating conditions. The production of the green synthesized AgNPs was maximized via the application of one-factor-at-a-time technique to optimize the different physicochemical factors influencing the biofabrication batch process. Different microscopic and spectroscopic techniques were employed to approve the purity and stability of the prepared AgNPs. As much as to our knowledge, this study can be considered as the first to explore the feasibility and profitability of the green synthesis of AgNPs. It was proved by performing an integrated preliminary cost analysis for the bioreductant and AgNPs production batch processes. Moreover, to make the fabrication process more eco-friendly; according to our information, this study is the first to reach zero-waste discharge, via the valorization of the fabrication process' spent wastes into activated carbon (AC), which is a valuable by-product with multiple applications.

Date and location of the research

The research has been conducted within the year 2019–2020, in Egyptian Petroleum Research Institute, October University for Modern Sciences and Arts and University of Nottingham.

Materials and methods

Water extract of the agro-industrial waste

Waste mandarin peels were provided from a nearby fruit drink shop. The methodology reported by El-Gendy et al. (2016) was followed to produce the mandarin peels' extract.

Optimization of the physicochemical factors that influence the phytogenesis of AgNPs

To investigate the influence of the process variables (illumination, initial pH, extract and precursor concentrations, mixing rate, reaction temperature and time) and to optimize the conversion of Ag^{+} ions into Ag^{0} NPs, one-factor-at-a-time optimization method (OFAT) was employed (Omran et al. 2018a). UV/Vis spectrophotometer (JASCO Analytical instruments, 8649 Commerce Drive, Easton, Maryland 21601–9903, USA) was employed to follow the phytoreduction of silver ions into AgNPs. Here, the concentration of the produced AgNPs was calculated based on a previously performed calibration curve with concentrations ranging from 35 to 600 mg L^{-1} AgNPs (Omran et al. 2018b).

Purification and characterization of the phyto-fabricated AgNPs

Purification of the phytosynthesized AgNPs was performed via centrifugation with a speed rate of 10,000 rpm for 30 min. The resultant powder was dehydrated overnight in an oven adjusted at 50 °C till reaching a fixed weight to calculate the yield. Then, the full characterization of

the prepared AgNPs was done according to Omran et al. (2018a).

Preliminary cost analysis

In an attempt to predict a preliminary cost for both the hot water extract of mandarin peels (Fig. 1a) and the green synthesized AgNPs (Fig. 1b), operational cost analysis for the production processes was performed. It is based on the cost of the raw materials and the energy consumed during the processes. According to the commercial pricing of the Egyptian Ministry of Electricity, the price of the needed and supplied electricity for the equipment was considered as 0.04 US$ per kW.h. The operational cost was calculated based on the consumed power (kW/h) during the batch synthesis processes of both MPE and AgNPs (Fig. 1).

Extraction process

Tap water and mandarin peels were considered as raw materials. Double distilled water produced via a water distiller unit (10 L h^{-1}) was used for the batch synthesis process. Based on the working capacity of 1 h, double distilled water volumetric cost was calculated using Eq. 1:

$$C_{\mathrm{w}} = \left(P_{\mathrm{r}} * C_{\mathrm{e}} * t\right) + C_i \quad (1)$$

where C_{w} represents the cost of the produced double distilled water (US$), P_{r} represents the rated power of the equipment (kW), C_{e} represents the cost of consumed electric power (US$ per kW.h), t represents the processing time (h) and C_i represents the cost of the feedstock, i.e., the tap water (US$). As a result, double distilled water volumetric cost was concluded to be 0.03 US$ per L. For the extract prepration; 250 mL double distilled water per 100 g mandarin peels were used in a 3 h batch process at 100°C. Approximatly, 150 mL water were then recovered using a rotary evaporator and finally, the produced extract condensed solution was filtered and dried to a constant, in a drier set at 80°C for 12 h. The operational cost for both water bath and drier units was calculated based on Eq. 2. The required operational electrical power for the production of 18 g of MPE from 100 g mandarin peels was concluded to be 0.825 kW.h and 9.6 kW.h for both water bath and drier units, respectively. Thus, for the production of 1 kg extract (i.e., bioreductant), 45.83 kW.h and 9.6 kW.h were required for water bath and drier units, respectively, in addition to 5.6 L double distilled water. Consequently, the calculated operational cost for the extraction process of 1 kg of the bioreductant using Eq. 2 was 1.92 US$ and 0.4 US$ for water bath and drier units, respectively. Finally, the operational production cost of 1 kg of MPE was concluded to be 3.1 US$ using Eq. 2.

$$C = f_i\left[\sum C_n\right] \quad (2)$$

where C represents the total operational costs, f_i represents the indirect cost factor (greater than 1) and C_n represents the summation of the total working capital costs.

Estimation for the cost analysis of the suggested AgNPs batch phytosynthesis process

Cost estimation similar to that of mandarin peels' hot water extraction process was applied to the green genesis of AgNPs using MPE. A simple flowchart for the suggested phytosynthesis of AgNPs using the MPE is illustrated in (Fig. 1b). $AgNO_3$, MPE and distilled water were considered as the feedstock for the production process of AgNPs. The process included the preselected optimum operating conditions, separation (i.e., centrifugation) and drying operations.

Valorization of the spent waste mandarin peels into activated carbon

The mandarin peels spent waste withdrawn out from the bioreductant production batch process was dried out in an oven overnight at 105 °C. Then, it was ground by ball milling (Model: RETSCH PM-400) at an acceleration rate of 350 rpm for 1 h. Afterward, the obtained powder was valorized into AC according to the method reported by El-Salamony et al. (2017). Here, the conversion was approximately 80%, indicating the simplicity and profitability of the applied preparation process. Finally, the prepared AC was characterized according to Omran et al. (2019).

Results and discussion

Production yield of MPE

Hot water extraction of mandarin peels yielded about 18 g of MPE per 100 g of dried mandarin peels. For over-stimulating the usage of mandarine waste peels and reaching the point of zero waste, the residuals of the extraction process (i.e., spent waste mandarine peels) were suggested to be further upcycled into biogas, biofertilizer and/or activated carbon (Fig. 1a). This manuscript focuses on AC.

Visual inspection of color change

The preliminary indication for the formation of AgNPs was the change in coloration from yellow to dark brown as revealed in Fig. 2a. Notably, no change in color took place in the control set (i.e., MPE solution without the addition of

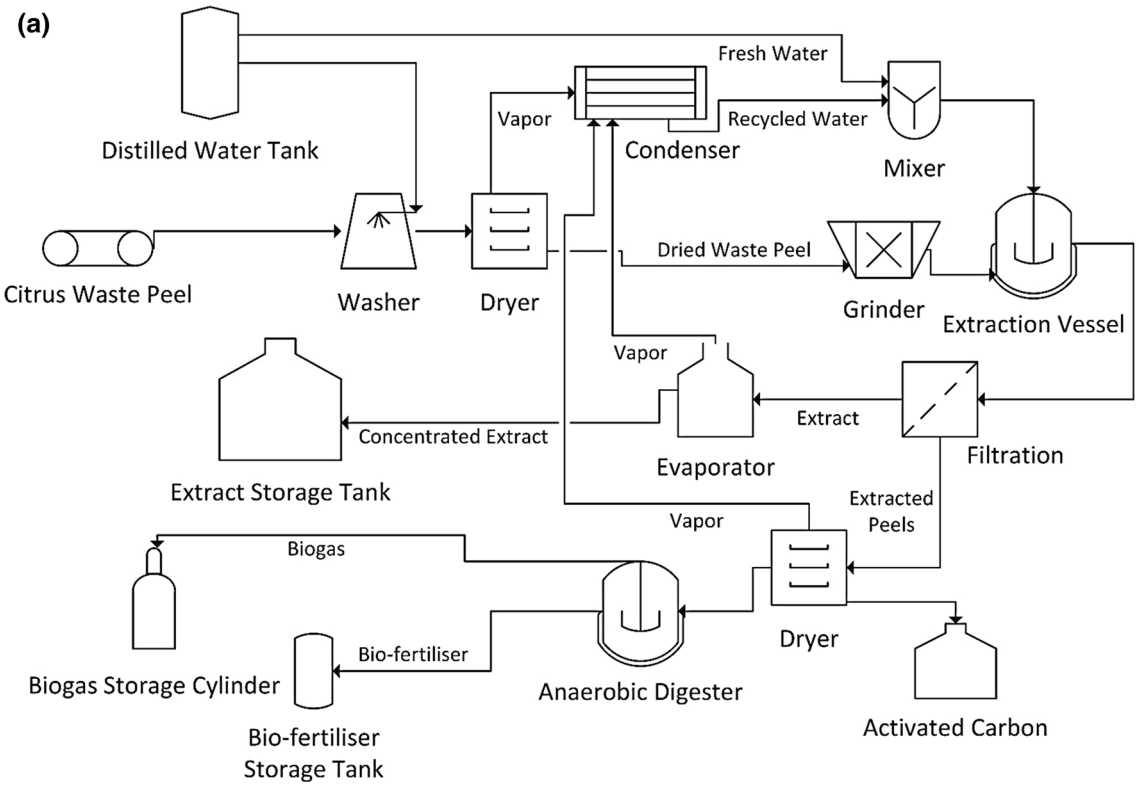

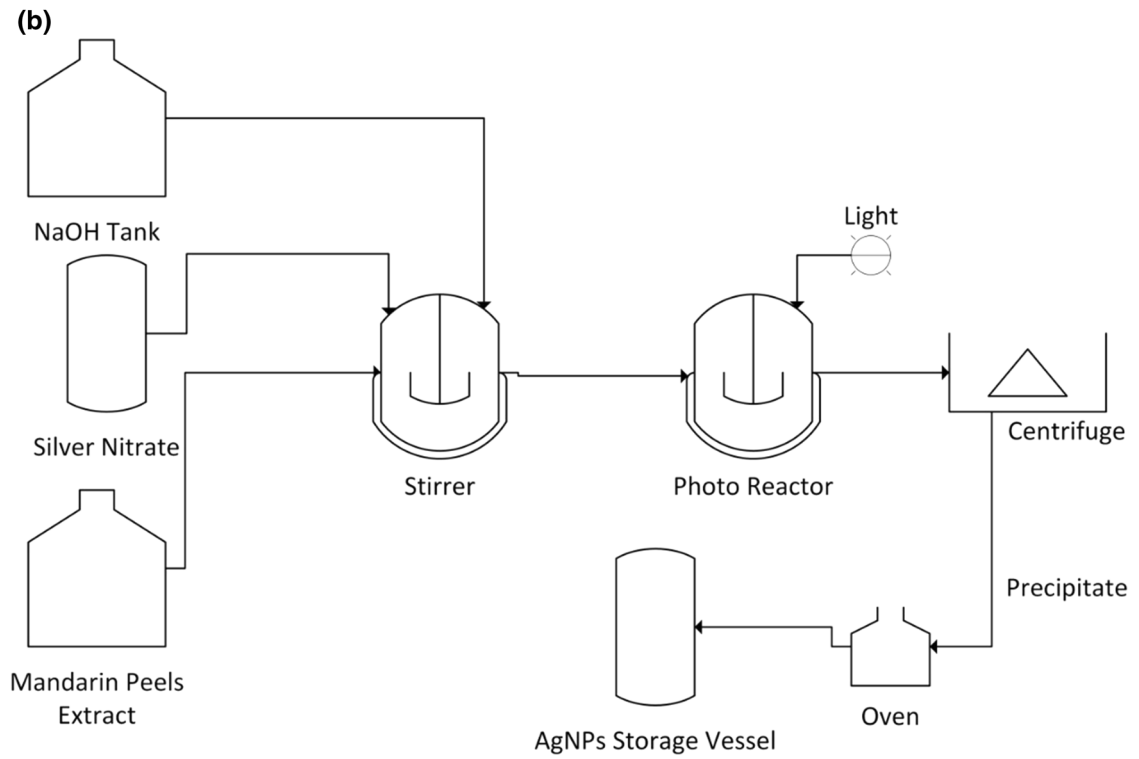

Fig. 1 A scheme for the MPE preparation process (**a**), flowchart showing the process of green synthesis of AgNPs by MPE (**b**)

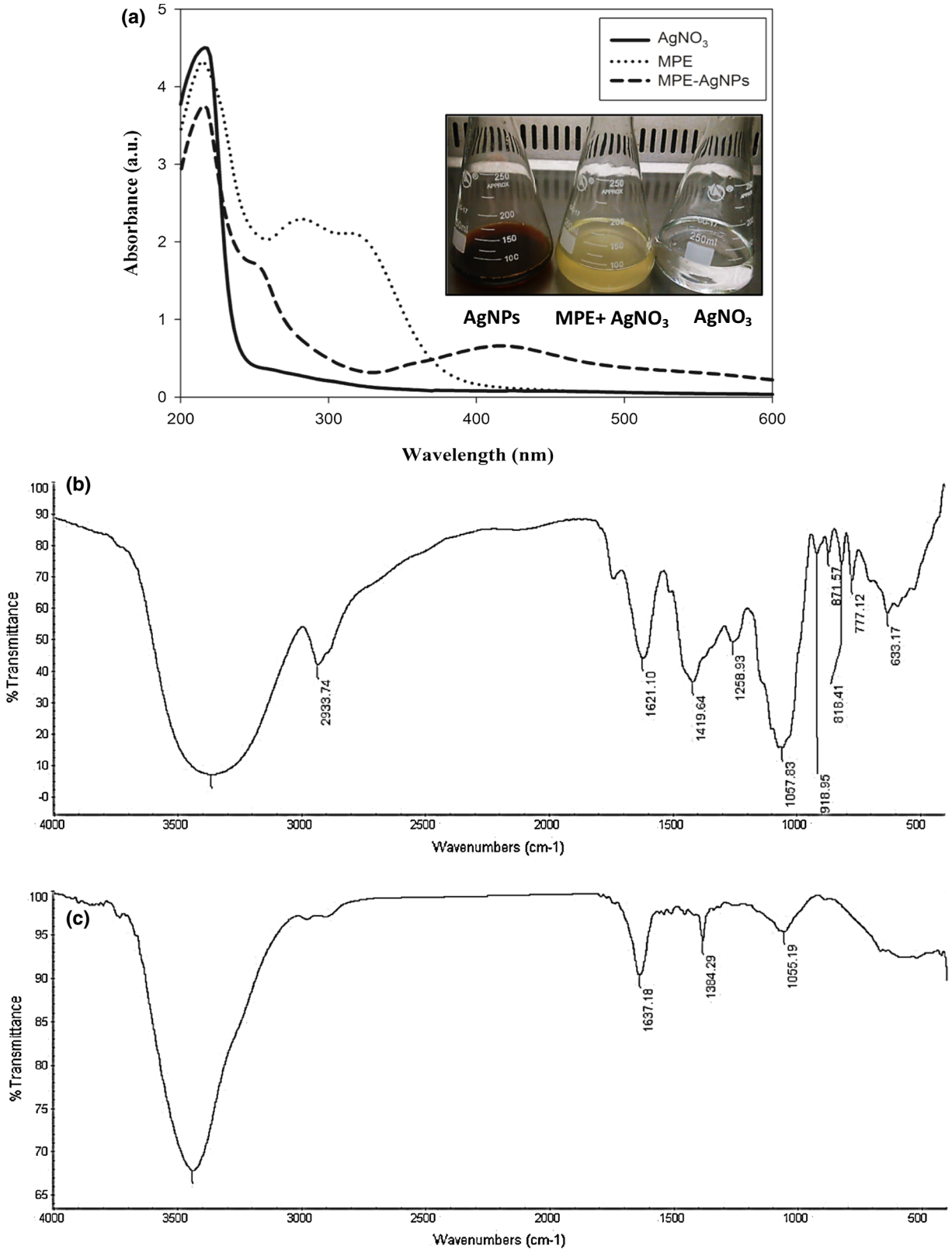

Fig. 2 Overlaid UV/Vis spectra of $AgNO_3$, MPE and AgNPs during preliminary screening of AgNPs green synthesis (**a**), FTIR spectra of MPE (**b**) and green synthesized AgNPs (**c**)

$AgNO_3$). The reason behind the color change is the excitation of AgNPs' free electrons, which in turn results in phase fluctuation and refers to surface plasmon resonance (SPR).

Spectrophotometric analysis

The major components of MPE as reported by Omran et al. (2013) are terpenoids (e.g., limonene), furanone (e.g., 2,4-dihydroxy-2,5-dimethyl-3(2H)-furan-3-one), sugar derivatives (e.g.2,3-dihydro-3,5-dihydroxy-6-methyl-4H-pyran-4-one (DDMP), 5-hydroxymethylfurfural (HMF), saturated fatty acids (e.g., tetradecanoic, pentadecanoic and hexadecanoic acids), benzoic acid and other phenolic compounds (e.g., 2-methoxy-5-(1-propenyl)phenol and 2-methoxy-4-vinyl phenol (MVP)).

The UV spectrum of the MPE solution (Fig. 2a) reveals the existence of the 228 nm band, which might indicate the presence of high concentrations of alkylbenzenes (El-Gendy et al. 2009). Besides, peaks ranging from 256 to 320 nm would confirm the presence of aromatic and phenolic compounds. According to Parlinska-Wojtan et al. (2016), terpenoids were recognized by the presence of two peaks at 280 and 320 nm. The production of AgNPs was confirmed via the presence of AgNP's distinctive SPR at 438 nm and the disappearance of the characteristic peak of $AgNO_3$ at 216–220 nm. Such observed disappearance in MPE characteristic peaks with the production of AgNPs would indicate the bioreduction of Ag^+ to Ag^0 by the biological constituents of MPE which would have functioned as natural reductants, stabilizers and capping agents (Durán et al. 2005; Trivedi et al. 2014; Omran et al. 2018a).

Fourier transform infrared (FTIR) spectroscopic analysis was performed to predict the possible interactions between both silver ions and the biological constituents of the MPE. The FTIR spectrum of MPE (Fig. 2b) demonstrates the distinctive absorption peak of the hydroxyl (O–H) groups at 3365 cm^{-1}. The C–N stretching of amine groups was detected by the appearance of a peak at 2933 cm^{-1}. The strong peak at 1621 cm^{-1} is assigned to the bending vibration of the aromatic C = C. The bands appearing between 1419 and 1616 cm^{-1} indicate the existence of phenolic groups. The peak at 1258.08 cm^{-1} is assigned to C–N stretching in amines. The sharp band at 1057 cm^{-1} reveals the presence of ether bonds. The absorption band at 918 cm^{-1} is assigned to the alkene bending of the C–H functional group. The weak bands at 818 and 871 cm^{-1} are assigned to the C = C bending in alkenes and the bending vibrations of –O–H, respectively. The bands noticed at 777 cm^{-1} and 633 cm^{-1} are assigned also for the C-H bending and stretching in aromatics and alkenes, respectively. Concisely, FTIR results prove the existence of –OH, –C = O, C–O acidic stretching, C = C aromatics, C–N aliphatic amine stretching and C-H alkane stretching. The FTIR spectrum of the prepared AgNPs (Fig. 2c) expresses a shift in certain absorption peaks: 3365, 1621, and 1057 cm^{-1}. It shows also the disappearance of 2933, 1419 and 1258 cm^{-1}; besides, the peaks ranged between 918 and 633 cm^{-1}. Nevertheless, it assures the appearance of a peak at 1384 cm^{-1}.Consequently, the FTIR spectra illustrate the capability of MPE to act as a reductant, a stabilizer and a capping agent (Fig. 3). For instance, hydroxyl groups present in polyphenols act as reductants via the charge transfer mechanism. Also, vitamins like ascorbic change the atmospheric oxygen into the water. This reaction is accelerated in the presence of metallic ions and illumination. The reducing power of ascorbic acid is enhanced by its oxidation to dehydroascorbic acid, thus aiding in the formation of AgNPs. Some other phenolic compounds such as terpenoids, alkaloids and some coenzymes act also as reducing agents. Furthermore, coenzymes such as nicotinamide adenine dinucleotide (NAD), which appear in two types, namely NADH and NAD^+, might be also involved. NAD^+ is an oxidizing agent and becomes reduced by acting as an electron acceptor, while NADH becomes an electron donor and aids in electron transportation during redox reactions. Oxidation of hemiacetal and hydroxyl groups to carbonyl and acetate groups helps in the reduction of Ag^+ ions. Additionally, amino acids' free carboxylate ions or amine groups could bind to AgNPs and hence act as capping and stabilizing agents.

Process optimization

The size and shape of AgNPs control the SPR position and its width (Wilcoxon et al. 1998). The increase in the size of AgNPs shifts the absorption spectra toward longer wavelengths (i.e., redshift), while the decrease in size of AgNPs shifts the SPR toward lower wavelengths (i.e., blueshift) (Yang and Li 2013). Thus, the observed absorption peaks within the range of $\lambda_{420–426\ nm}$ proved the decrease in the size of the green synthesized AgNPs.

Effect of temperature

The reaction temperature expresses a substantial influence (Fig. 4a). The reaction mixture showed lighter brown coloration with a low pronounced SPR peak at 20 and 40 °C, while at 30 °C, a denser brown color occurred with the expression of a maximum absorption sharp narrow peak of 342 mg L^{-1} AgNPs at λ_{426nm}. But at a higher temperature (50 °C), a flat broadened band was obtained with the lowest occurrence of AgNPs concentration (188 mg L^{-1}). At higher temperatures, faster nucleation occurs and silver particles grow bigger,

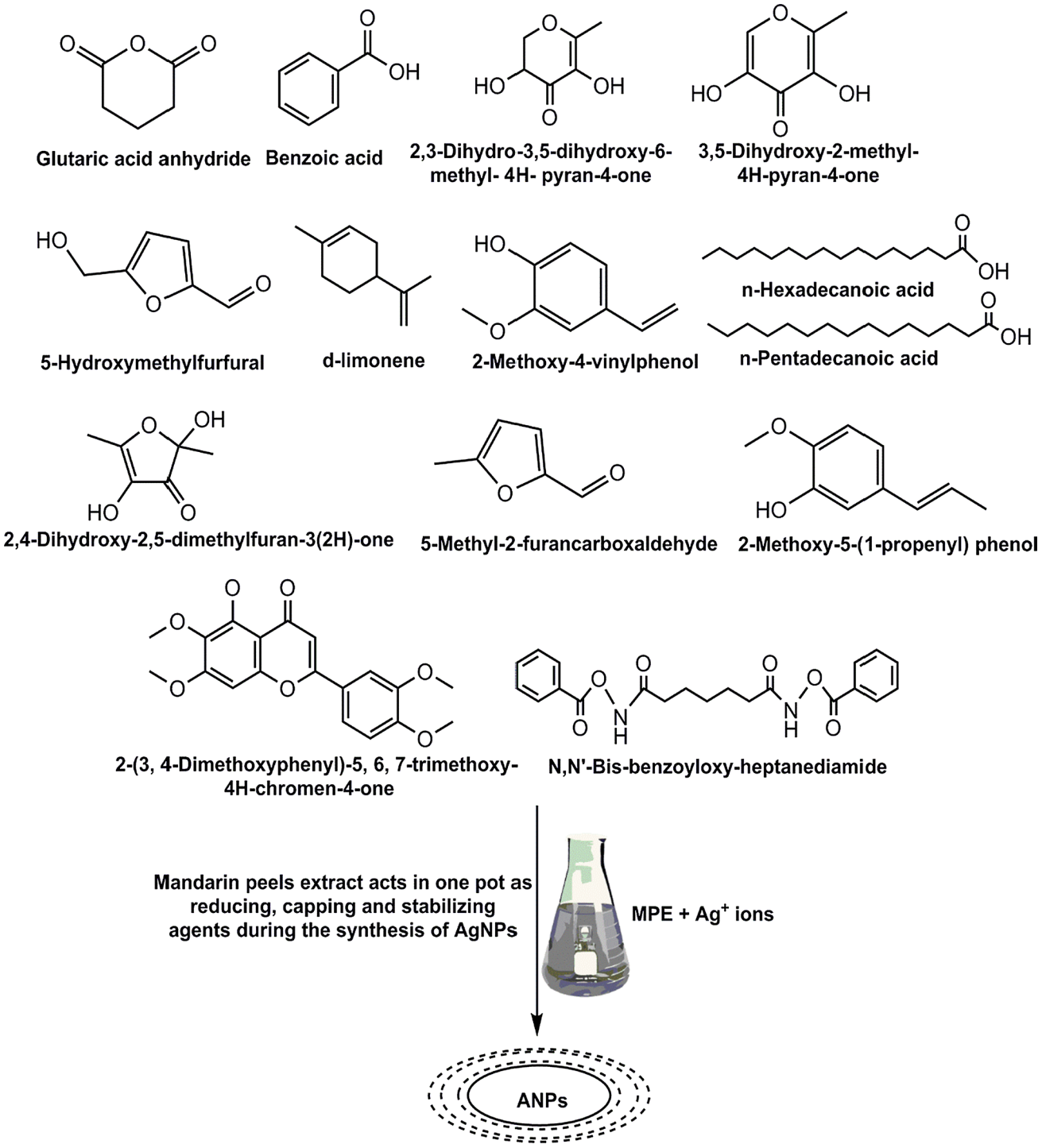

Fig. 3 Elucidated possible mechanism for the green synthesis of AgNPs

which consequently leads to broadening of the SPR peak and its redshift (i.e., to longer wavelength). Gopalakrishnan et al. (2016) demonstrated that 30 °C is the optimum temperature for synthesizing AgNPs via the aqueous *Azadirachta indica* (neem) flower extract.

Effect of illumination and darkness

Figure 4b proves that the absorption peak of the AgNPs prepared under illumination exceeds that of dark condition, recording 1225 mg L^{-1} and 1177 mg L^{-1}, respectively. This is ascribed to the existence of a high number of

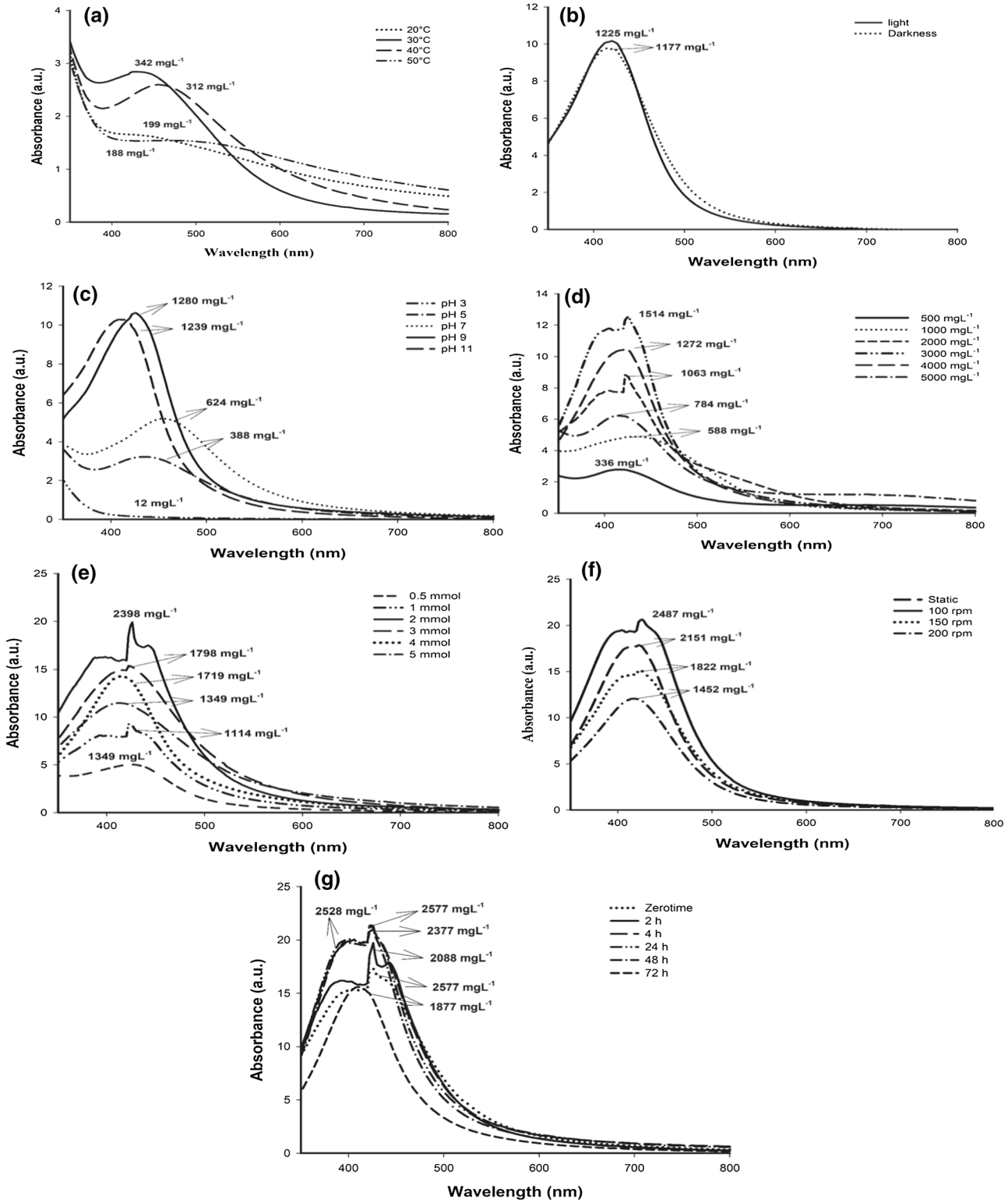

Fig. 4 Effect of temperature **a** and illumination and darkness **b** pH **c** and mandarin peel extract (MPE) concentration **d** $AgNO_3$ concentration **e** mixing speed **f** and reaction time **g** on green synthesis of AgNPs, respectively

photons under fluorescent light, which enhances the bioreduction reactions and promotes the formation of AgNPs (Srikar et al. 2016). Moreover, the nucleophilic carboxylic groups can easily bind to Ag^+ via the partial transfer of electrons (Nam et al. 2008).

Effect of reaction pH

The synthesis of AgNPs was inhibited under acidic conditions (Fig. 4c). At acidic pH (3–5), faint brown coloration occurred and a very low broad SPR peak of AgNPs was obtained. By increasing the initial pH from neutrality to basic conditions, the sharp absorption peak of AgNPs started to increase until it reached its maximum absorbance at pH9, recording 1280 mg L^{-1} at $\lambda_{426\ nm}$, and then decreased at higher pH. This behavior is attributed to the ionizing of phenolic compounds and furanone. In alkaline conditions, there is a high amount of hydroxide ions promoting the reduction and capping processes, while the vice versa occurs in acidic conditions since the functional groups in the extract are positively charged, and consequently, the reduction capacity of these groups decreases and the capping efficiency declines; thus, the stability of the formed NPs decreases. So, at acidic conditions, nucleation of the nanoparticles vigorously occurs, and larger NPs, even micro- and/or macro-ones formed. But in alkaline conditions, electrostatic repulsion arises between the green synthesized NPs, aggregations diminished and smaller and more stable AgNPs formed. As reported by Khalil et al. (2017), the main effect of pH is its capability to change the charge of the biomolecules and hence alter their reducing and capping power. According to Gopalakrishnan et al. (2016) at acidic pH, the synthesis of AgNPs decreases, and the formation of large-sized AgNPs occurs. Further, Vanaja et al. (2013) and Jain and Mehata (2017) reported that alkalinity is more preferred in the green synthesis of NPs. Moreover, Rashidipour and Heydari (2014) and Verma et al. (2017) demonstrated that pH 9 is the best pH for the biological fabrication of AgNPs via the water extracts of oak fruit hull (Jaf) and *Solanum nigrum* leaves.

Effect of different concentrations of MPE

MPE concentration greatly influences the green synthesis of AgNPs (Fig. 4d). The intensity of SPR increases with the increase in MPE concentration recording its maximum 1514 mg L^{-1} at $\lambda_{426\ nm}$ using 3000 mg L^{-1} MPE. But at higher MPE concentrations, a decrease in AgNPs-SPR absorption occurs. Thus, this indicates a sufficient extract concentration leads to an acceleration in the bioreduction of Ag^+ and the successive nucleation of the Ag nuclei, which promotes the preparation of small-sized AgNPs. Gopalakrishnan et al. (2016) reported that optimum extract concentration is necessary for the preparation of NPs, where a lesser or greater volume of bio-extract expresses low SPR of AgNPs indicating the incomplete synthesis of NPs. According to Liu et al. (2010) and Amin et al. (2012) beyond a certain limit, the biomolecules (i.e., phenolics, alkaloids, sugars, etc.) in a certain biological source stop to play their capping role and lead to a phenomenon called Ostwald ripening causing an increment in NPs size.

Effect of different concentrations of $AgNO_3$

Figure 4e shows an increase in the SPR of the biosynthesized AgNPs with the increase in the concentration of the $AgNO_3$ precursor recording its maximum 2393 mg L^{-1} at 2 mmol $AgNO_3$. However, a further increment in $AgNO_3$ concentration ≥ 3 mmol leads to a decrease in the AgNPs concentrations. Ibrahim (2015) reported an optimum $AgNO_3$ concentration of 1.75 mmol for the green synthesis of AgNPs using banana peel extract. Based on LaMer's theory, Ag^+ concentration acts as the driving force for accomplishment of AgNPs formation via three successive steps: nucleation, growth and completion. Thus, to accurately synthesize uniform AgNPs, homogeneous nucleation is needed. However, for the synthesis of AgNPs, the optimal monomer concentration (Ag^+) should exceed the energy barrier, i.e., the Gibbs free energy of spherical seed formation (LaMer and Dinegar 1950).

Effect of different mixing speeds

The maximum absorption peak of 2487 mg L^{-1} AgNPs was recorded at 100 rpm (Fig. 4f). Increasing the reaction speed results in speeding up of the mixing of reactants, which in turn induces the process of bioreduction. However, it is worth noting that beyond a certain speed, a rise in the reaction mixture turbulence takes place and results in minimizing the production of AgNPs. A similar observation was reported for the green genesis of AgNPs via sweet orange peels' hot water extract (Wen et al. 2017).

Effect of reaction time

The conversion of Ag^+ ions into its NPs state occurred fairly rapidly, recording maximum SPR of 2577 mg L^{-1} within a reaction time of 4 h (Fig. 4g). Then, it kept steady without any change in peak wavelength for up to 24 h. But at longer reaction time, the absorption peaks start to decrease, recording 2377 mg L^{-1} and 2088 mg L^{-1} at 48 h and 72 h, respectively, due to the increase in aggregations. The observed rapid reaction time in this study is considered as an advance toward achieving the goal to compete with the chemical synthesis of AgNPs. Basavegowda and Lee (2013) reported that the best time for synthesizing AgNPs via *Satsuma* mandarin (*Citrus unshiu*) and *Gymnema sylvestre* leaf extract is 72 h. However, Rashidipour and Heydari (2014) reported 4 h as the optimum time for green synthesis of AgNPs using the aqueous extract of (*Olea europaea*) olive leaf.

Yield of AgNPs at elucidated optimum operating conditions

The yield of MPE-AgNPs reached 0.25 g per 100 mL, at the following optimum operating conditions: 3000 mg L^{-1} MPE, 2 mmol $AgNO_3$, initial pH 9, 30 °C, 100 rpm, under illumination and 4 h.

Characterization of the green synthesized AgNPs

The main average size of the green synthesized AgNPs is about 53.9 nm as revealed by DLS-analysis (Fig. 5a), with a polydispersed index (PdI) of 0.197 and intercept of 0.911. The obtained PdI value is less than 0.5 assuring the monodispersity of the green synthesized AgNPs (Vasquez et al. 2016). The zeta potential of the dispersed AgNPs was recorded as -22.3 mV (Fig. 5b). This proves the high stability of the prepared AgNPs (Anandalakshmi et al. 2016; Wen et al. 2017). Zeta potential confirms the existence of a negative charge on the surface of the AgNPs. Anandalakshmi et al. (2016) reported that aggregation was reduced by the effect of the coulombic repulsion forces due to the presence of surface negative charge and hence aided in producing stabilized AgNPs. According to Heydari and Rashidipour (2015), when zeta potential values are greater than +25 mV or lesser than −25 mV, high levels of stability can be attained. The zeta potential obtained in this study is due to the existence of MPE biomolecules which capped and stabilized the synthesized AgNPs. EDX illustrated the presence of signals near 3.68 keV (Fig. 5c). Kumar and Kathireswari (2016) reported that peaks between 3 and 4 keV resemble the binding energy of Ag. Moreover, the additional peaks for carbon and oxygen peaks appearing in the spectrum are due to the bioreductant molecules surrounding the surface of AgNPs (Banala et al. 2015). Four characteristic XRD peaks observed in Fig. 5d correspond to the face-centered cubic structure of AgNPs. The reflection peaks are (111), (200), (220) and (311) that plane at 2θ angles of 38.01°, 44.06°, 64.645° and 77.41, respectively. This aligned well with the unit cell structure of silver lines (JCPDS File No. 01-071-4613). Extra and unknown Bragg peaks were also observed, which are attributed to the existing bioreductant constituents. The average crystallite size (d) of the biosynthesized AgNPs was predicted using the Debye–Scherer equation (Omran et al. 2018a,b) and recorded to be ≈35 nm. AgNPs exhibited a spherical shape as illustrated from FESEM images (Fig. 5e). For observing further details about morphology, the HRTEM analysis was performed, which shows uniformly distributed, rounded/oval-shaped, nonagglomerated and well-dispersed AgNPs, with a size ranging from 10 to 19.10 nm (Fig. 5f). Moreover, the HERTM image reveals green synthesized AgNPs coated with an organic layer which acts as a stabilizer and as a capping agent that leads to the perfect dispersion of the AgNPs. It is worthy to mention that the average size of AgNPs measured by HRTEM is less than that measured by DLS. This is attributed to the consideration of the hydrodynamic diameter of NPs and capping protein agents in the calculations of DLS technique. Basavegowda and Lee (2013) reported the green synthesis of AgNPs using Satsuma mandarin (*Citrus unshiu*) peel extract with a size range of 5–20 nm, while Jasuja et al. (2014) reported the green synthesis of spherical-shaped AgNPs, with a size average of 5–50 nm by the agro-industrial waste peel extract of *Punica granatum*.

Estimated cost analysis for the batch green synthesis process of AgNPs

According to Eqs. 1 and 2, the operational production cost of green synthesized AgNPs using MPE was concluded to be 19 US$ per 2.5 g of AgNPs. It is taken into consideration that the global price of the chemically synthesized AgNPs is 70 US$ per 2.5 g of AgNPs (US Research Nanomaterials, Inc., the advanced nanomaterials provider). This would give an income of approximately 51 US$ per 2.5 g of AgNPs. Consequently, these results prove the eco-feasibility of the valorization of mandarin waste peels into AgNPs.

Characterization of the prepared mandarin peels-derived AC

The valorization of the spent waste mandarin peels into AC has been achieved (Fig. 6a) and donated the name MP-AC. The FTIR analysis of the ground spent waste mandarin peels (Fig. 6b) reveals a band at 3400 cm^{-1} of the O–H stretching carboxylic group. The peak observed at 2925 cm^{-1} is

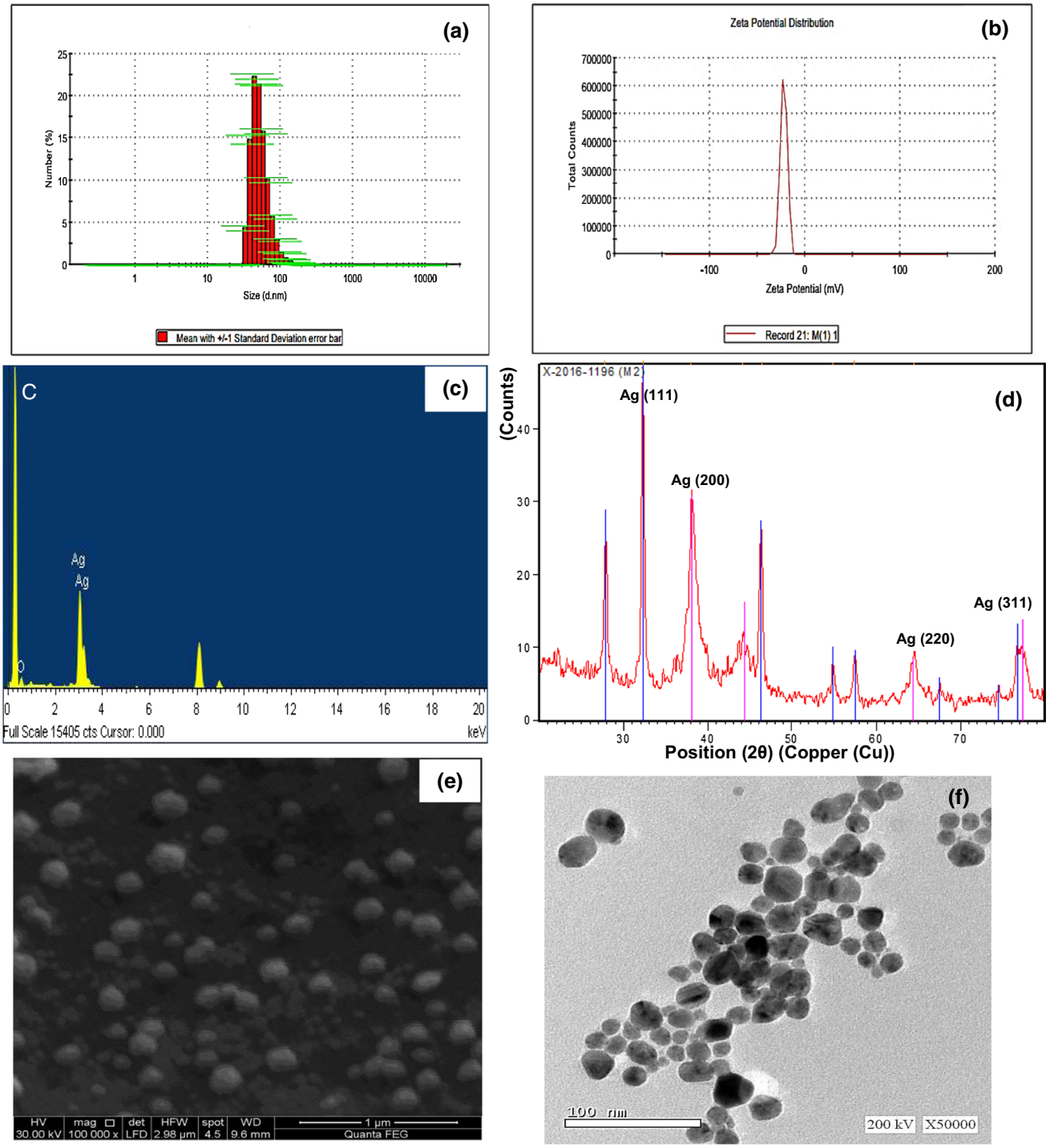

Fig. 5 AgNPs characterization: particle size distribution by dynamic light scattering (DLS) (**a**); zeta potential measurement (**b**); energy-dispersive X-ray (EDX) spectra (**c**); X-ray diffraction (XRD) pattern (**d**); field emission scanning electron microscope (FESEM) micrograph (**e**); and high resolution transmission electron microscope (HRTEM) image (**f**)

assigned to the C–H methyl and methylene groups. The band appearing at 1746 cm^{-1} is assigned to C = O and C–O stretching of phenolic ester, carboxylic acid and conjugated ketonic structures. The peaks at 1626 cm^{-1} and 1518 cm^{-1} are indicative of conjugated C = C phenyl rings and C = C aromatic ring stretching vibration, respectively, while the peak at 1445 cm^{-1} corresponds to C–H in-plane bends. The peak at 1370 cm^{-1} is indicative of symmetrical stretch nitro compounds. Aliphatic acid group vibration at 1272 cm^{-1} is attributed to the deformation vibration of C = O and

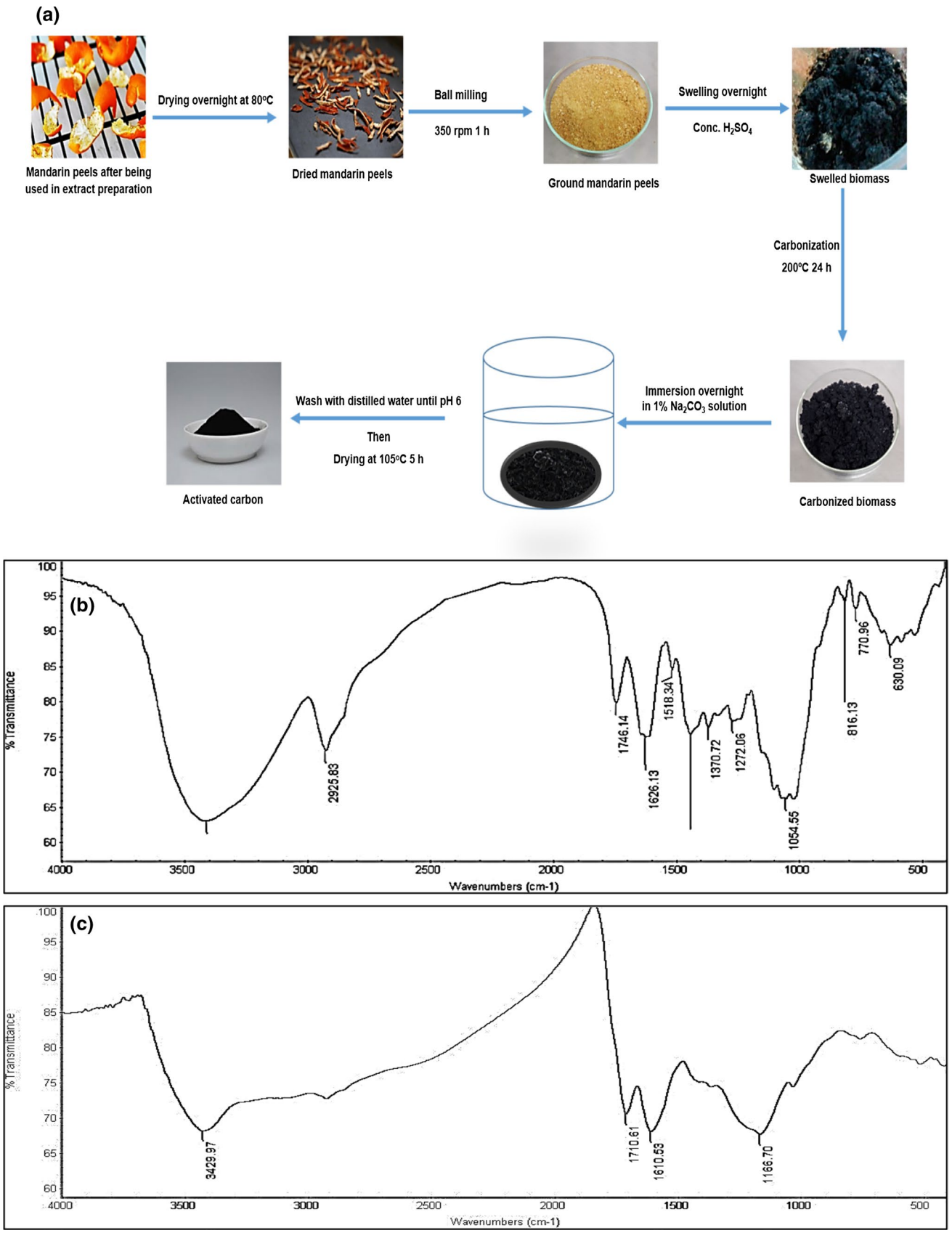

Fig. 6 Preparation steps of spent waste mandarin peels derived activated carbon (MP-AC) (**a**), FTIR spectra of ground spent waste mandarin peels (**b**) and the prepared MP-AC (**c**)

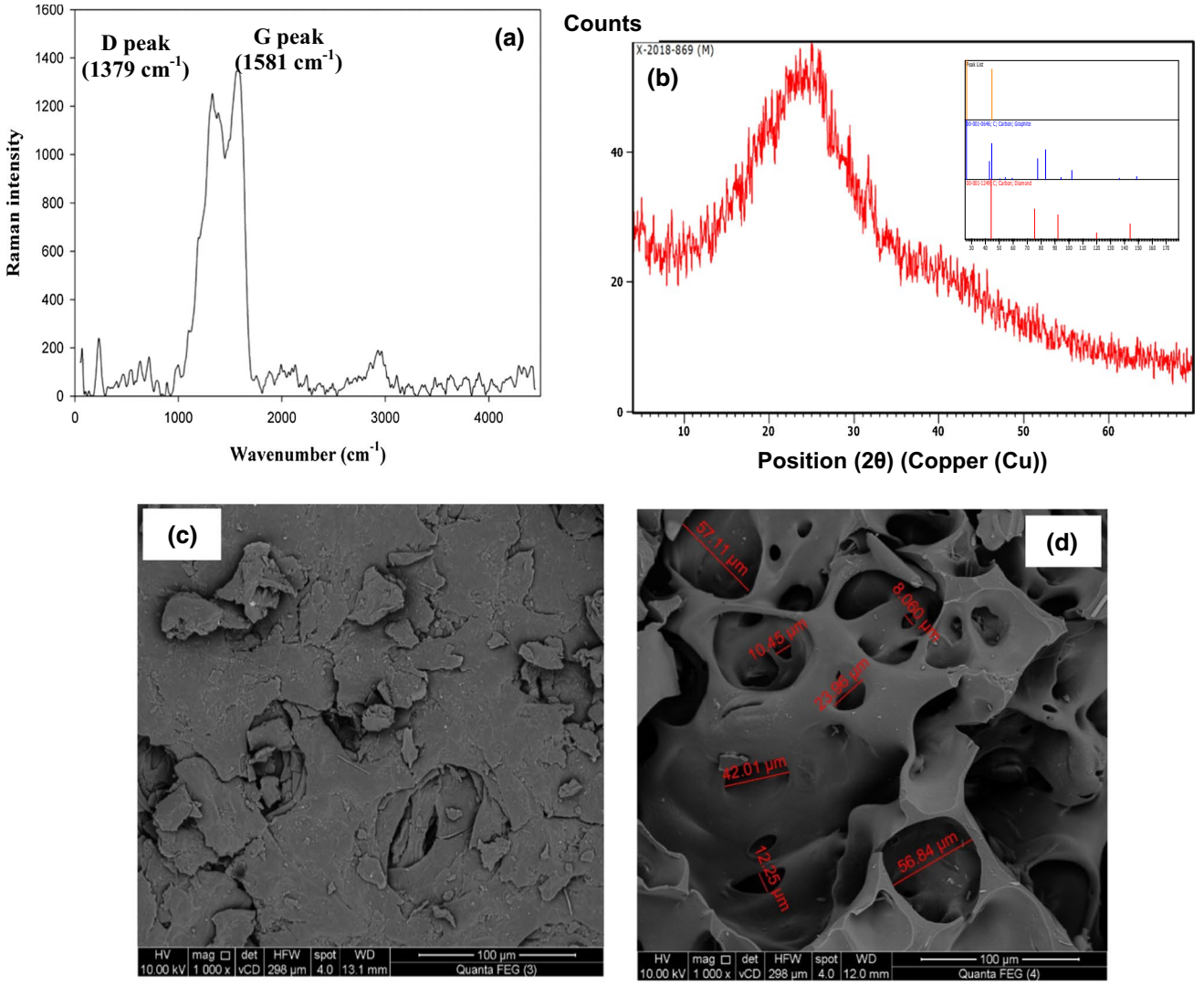

Fig. 7 Raman spectrum of prepared MP-AC (**a**), XRD pattern of the MP-AC (**b**), field emission scanning electron microscope (FESEM) micrographs of ground spent waste mandarin peels (**c**) and MP-AC (**d**)

stretching formation of –OH of carboxylic acids and phenols. The peak at 1054 cm^{-1} corresponds to a secondary alcohol, C–O stretch. Peaks at 816 and 770 cm^{-1} are indicative of strong bend C–H phenyl rings and aromatic C–H bending, respectively. On the other hand, four major peaks were identified in the FTIR analysis of the MP-AC (Fig. 6c). A strong band detected at 3429 cm^{-1} belongs to vibrations of OH-groups. The band appearing around 1710 cm^{-1} is assigned to C = O and C–O stretching and attributed to the phenolic ester, carboxylic acid and conjugated ketonic structures. The band appearing at 2929 cm^{-1} is attributed to the C–H methyl and methylene groups. The band appearing around 1610 cm^{-1} is assigned to conjugated C = C phenyl rings. The band appearing around 1166 cm^{-1} is assigned to C–O of carboxylic acid, phenols and esters. Other minor peaks found include the following: those around 1239 cm^{-1} are fingerprints of O–H of alcohol and carboxylic acid bending, while the peak at 1028 cm^{-1} corresponds to a secondary alcohol, C–O stretch. Figure 7a shows the Raman pattern of the MP-AC, where the *D* band corresponds to the frequency of the amount of carbon lattice disorders and is linked to the degree of sp^3 hybridization, which is approximately at 1379 cm^{-1}, while the *G* band of the graphitic network, first-order scattering which is linked to the extent of sp^2 hybridization (either in aromatic rings or chains), is at 1581 cm^{-1}. The level of sp^2 hybridization $I_D/I_G = 0.4743$ is less than

one, indicating crystalline graphite (EL-Salamony et al. 2017). The results obtained from the XRD reveal the presence of broad reflections of typically amorphous material at 2θ angles of 26° and 44°, which are in a match with the unit cell structure of carbon (JCPDS File No. 00-001-0646 and 00-001-1249), thus indicating the crystallite graphite (Fig. 7b). The BET surface area is evaluated to be 890 m^2/g, the BJH pore volume is 0.173 cc/g and the BJH pore radius is estimated to be 1.92 nm. The FESEM micrographs of ground spent waste mandarin peels show a smooth surface (Fig. 7c), while the FESEM micrographs of the prepared MP-AC (Fig. 7d) clearly reveal the occurrence of dramatic effects on the solid surface of mandarin peels after activation, where a rough surface with pores of different sizes and shapes is observed. The holes and cavities found on the surface are due to the evaporation of H_2SO_4 during activation, creating empty spaces. The pore sizes as revealed from the FESEM images range between 8.01 and 57.11 µm. Rahman et al. (2012) prepared AC from waste palm shells and reported that the permeating agents like sulfuric acid aid in creating pores and reducing the appearance of tars and other liquids blocking the pores and preventing the creation of porous structures.

Conclusion

This study reveals an integrated process for reaching the point of zero-waste and fashions valuable insights into the importance of upcycling of waste mandarine peels. Hot water MPE shows an exceptional performance as bioreductant, biostabilizer and biocapping agent for biological fabrication of AgNPs. It yielded 2.5 g/L pure, highly stable, well-dispersed and non-agglomerated spherical-shaped AgNPs, with an average size of 14.6 nm. The preliminary cost analysis of the upcycling of mandarin waste peels into green synthesized AgNPs reveals the profitability of the proposed green synthesis relative to the global prices of the chemically synthesized AgNPs, recording 19 and 70 US$ per 2.5 g of AgNPs, respectively. Moreover, the valorization of the disposed spent waste mandarin peels after the green fabrication of AgNPs, into activated carbon with different valuable applications adds new value for such spent waste. Further work is now going to investigate the feasibility of upgrading the spent waste mandarin peels into other valuable products, such as animal fodder, fertilizer and feedstock for biofuels, biodiesel, bioethanol, biogas and solid fuel pellets.

Acknowledgements The authors wish to thank all who assisted in conducting this work.

References

Ahmad H, Rajagopal K, Shah AH (2016) The green route of silver nanotechnology: phytosynthesis and applications. Int J Nano Dimens 7:97–108

Ali HR, Nassar HN, El-Gendy NSh (2017) Green synthesis of α-Fe_2O_3 using citrus reticulum peels extract and water decontamination from different organic pollutants. Energy Source Part A 39:1425–1434

Amin M, Anwar F, Janjua MRSA, Iqbal MA, Rashid U (2012) Green synthesis of silver nanoparticles through reduction with *Solanum xanthocarpum* L. berry extract: characterization, antimicrobial and urease inhibitory activities against *Helicobacter pylori*. Int J Mol Sci 13:9923–9941

Anandalakshmi K, Venugobal J, Ramasamy V (2016) Characterization of silver nanoparticles by green synthesis method using Pedalium murex leaf extract and their antibacterial activity. Appl Nanosci 6:399–408

Apergis N, Bhattacharya M, Hadhr W (2020) Health care expenditure and environmental pollution: a cross-country comparison across different income groups. Environ Sci Pollut Res 27:8142–8156

Arya A, Mishra V, Chundawat TS (2019) Green synthesis of silver nanoparticles from green algae (*Botryococcus braunii*) and its catalytic behavior for the synthesis of benzimidazoles. Chem Data Collect 20:100190–100197

Banala RR, Nagati VB, Karnati M (2015) Green synthesis and characterization of *Carica papaya* leaf extract coated silver nanoparticles through X-ray diffraction, electron microscopy and evaluation of bactericidal properties. Saudi J Biol Sci 22:637–644

Basavegowda N, Lee LK (2013) Synthesis of silver nanoparticles using Satsuma mandarin (*Citrus unshiu*) peel extract: a novel approach towards waste utilization. Mater Lett 109:31–33

Czech A, Zarycka E, Yanovych D, Zasadna Z, Grzegorczyk I, Kłys S (2020) Mineral content of the pulp and peel of various citrus fruit cultivars. Biol Trace Elem Res 193:555–563

Duran N, Marcato PD, Alves OL, De Souza GI, Esposito E (2005) Mechanistic aspects of biosynthesis of silver nanoparticles by several *Fusarium oxysporum* strains. J Nanobiotechnol 3:1–7

El-Gendy NSh, Moustafa YM, Barakat MAK (2009) Evaluation of a bioslarry remediation of petroleum hydrocarbons contaminated sediments using chemical, mathematical and microscopic analysis. Int J Environ Stud 66:563–579

El-Gendy NSh, Hamdy A, Fatthallah NA, Omran BA (2016) Recycling of some domestic wastes to produce green corrosion inhibitors and biocides for sulfate reducing bacteria. Energy Source Part A 38:3722–3732

El-Gendy NSh, Hamdy A, Omran BA (2018) Thermal and surface studies on the corrosion inhibition of petroleum pipeline by aqueous extract of *Allium cepa* skin under acidic condition. Energy Source Part A 8:905–915

El-Salamony RA, Amdeha E, Ghoneim SA, Badawy NA, Salem KM, Al-Sabagh AM (2017) Titania modified activated carbon prepared from sugarcane bagasse: adsorption and photocatalytic degradation of methylene blue under visible light irradiation. Environ Technol 38:3122–3136

Fulekar J, Dutta DP, Pathaka B, Fulekar MH (2018) Novel microbial and root mediated green synthesis of TiO_2 nanoparticles and its application in wastewater remediation. J Chem Technol Biotechnol 93:736–743

Galanakis CM (2012) Recovery of high added-value components from food wastes: conventional, emerging technologies and commercialized applications. Trends Food Sci Technol 26:68–87

Ghosh PR, Fawcett D, Sharma SB, Poinern GEJ (2017) Production of high-value nanoparticles via biogenic processes using aquacultural and horticultural food waste. Materials 10:852–871

Gopalakrishnan V, Dhayalan M, Gandhi NN, Muniraj S (2016) Biosynthesis of silver nanoparticles using aqueous *Azadirachta indica* (Neem) flower extract-optimization, characterization and study of antimicrobial and anti-oxidant effects. Int J Innov Res Sci Eng Technol 5:11–21

Heydari R, Rashidipour M (2015) Green synthesis of silver nanoparticles using extract of oak fruit hull (jaft): synthesis and in vitro cytotoxic effect on MCF-7 cells. Int J Breast Cancer. Article ID 846743, 6 pages, http://dx.doi.org/10.1155/2015/846743

Ibrahim HMM (2015) Green synthesis and characterization of silver nanoparticles using banana peel extract and their antimicrobial activity against representative microorganisms. J Radiat Res Appl Sci 8:265–275

Jain S, Mehata MS (2017) Medicinal plant leaf extract and pure flavonoid mediated green synthesis of silver nanoparticles and their enhanced antibacterial property. Sci Rep 7:158867–158880

Jasuja ND, Gupta DK, Reza M, Joshi SC (2014) Green synthesis of AgNPs stabilized with biowaste and their antimicrobial activities. Braz J Microbiol 45:1325–1332

Kenawy IM, Mortada WI, Abou El-Reash YG, Mousa AA (2020) Preparation of lactic acid modified cellulose nanoparticles by microwave heating for preconcentration of copper from blood and food samples. Environ Sci Pollut Res 27:7256–7266

Khalil MMH, Ismail EH, El-Baghdady KZ, Mohamed D (2017) Green synthesis of silver nanoparticles using olive leaf extract and its antibacterial activity. Arab J Chem 7:1131–1139

Kheiralla ZH, Sh El-Gendy N, Ahmed HA, Shaltout TH, Hussein MMD (2018) One-factor-at-a-time (OFAT) optimization of hemicellulases production from *Fusarium moniliforme* in submerged fermentation. Energy Source Part A 40:1877–1885

Kumar KS, Kathireswari P (2016) Biological synthesis of silver nanoparticles (Ag-NPs) by *Lawsonia inermis* (henna) plant aqueous extract and its antimicrobial activity against human pathogen. Int J Curr Microbiol Appl Sci 5:926–937

LaMer VK, Dinegar RH (1950) Theory, production and mechanism of formation of monodispersed hydrosols. J Am Chem Soc 72:4847–4854

Liu Y, Zhang YA, Zhang M (2010) Green hydrothermal synthesis and characterization of CdO_2 nanoparticles. Mater Lett 64:1779–1781

Mahato N, Sinha M, Sharma K, Koteswararao R, Cho MH (2019) Modern extraction and purification techniques for obtaining high purity food-grade bioactive compounds and value-added co-products from citrus wastes. Foods 8:523. https://doi.org/10.3390/foods8110523

Mamma D, Christakopoulos P (2008) Citrus peels: an excellent raw material for the bioconversion into value-added products. Tree For Sci Biotechnol 2:83–93

Milik SM (2011) Master thesis. American University, Cairo

Mohamed RMA (2015) Chemical and biological evaluation of deterpenated orange and mandarin oils. Ph.D. disserattion, Al-Azhar University, Cairo, Egypt

Nam KT, Lee YJ, Krauland EM, Kottmann ST, Belcher AM (2008) Peptide mediated reduction of silver ions on engineered biological scaffolds. ACS Nano 2:1480–1486

Narasaiah BP, Mandal BK (2020) Remediation of azo-dyes based toxicity by agro-waste cotton boll peels mediated palladium nanoparticles. J Saudi Chem Soc 24:267–281

Nava OJ, Soto-Robles CA, Gomez-Gutierrez CM, Vilchis-Nestor AR, Castro-Beltran A, Olivas A, Luque PA (2017) Fruit peel extract mediated green synthesis of zinc oxide nanoparticles. J Mol Struct 1147:1–6

Omran BA, Fatthalah NA, El-Gendy NSh, El-Shatoury EH, Abouzeid MA (2013) Green Biocides against sulphate reducing bacteria and macrofouling organisms. J Appl Microbiol 7:2219–2232

Omran BA, Nassar HN, Fatthallah NA, Hamdy A, El-Shatoury EH, Sh El-Gendy N (2018a) Characterization and antimicrobial activity of silver nanoparticles mycosynthesized by *Aspergillus brasiliensis*. J Appl Microbiol 125:370–382

Omran BA, Nassar HN, Fatthallah NA, Hamdy A, El-Shatoury EH, Sh El-Gendy N (2018b) Waste upcycling of *Citrus sinensis* peels as a green route for the synthesis of silver nanoparticles. Energ Source Part A. 40:227–236

Omran BA, Nassar HN, Younis SA, El-Salamony RA, Fatthallah NA, Hamdy A, El-Shatoury EH, El-Gendy NSh (2019) Novel mycosynthesis of cobalt oxide nanoparticles using *Aspergillus brasiliensis* ATCC 16404—optimization, characterization and antimicrobial activity. J Appl Microbiol 128:438–457

Parlinska-Wojtan M, Kus-Liskiewicz M, Depciuch J, Sadik O (2016) Green synthesis and antibacterial effects of aqueous colloidal solutions of silver nanoparticles using camomile terpenoids as a combined reducing and capping agent. Bioprocess Biosyst Eng 39:1213–1223

Rahman MM, Awang M, Mohosina BS, Kamaruzzaman BY, Wan Nik WB, Adnan CMC (2012) Waste palm shell converted to high efficient activated carbon by chemical activation method and its adsorption capacity tested by water filtration. APCBEE Procedia 1:293–298

Rashidipour M, Heydari R (2014) Biosynthesis of silver nanoparticles using extract of olive leaf: synthesis and in vitro cytotoxic effect on MCF-7 cells. J Nanostruct Chem 4:112–118

Ravindran R, Jaiswal AK (2016) Exploitation of food industry waste for high value products. Trends Biotechnol 34:58–69

Sagar NK, Pareek S, Sharma S, Yahia EM, Lobo MG (2018) Fruit and vegetable waste: bioactive compounds, their extraction, and possible utilization. Compr Rev Food Sci 17:512–531

Santiago-De la Rosa N, González-Cardoso G, Figueroa-Lara JJ, Gutiérrez-Arzaluz M, Octaviano-Villasana C, Ramírez-Hernández IF, Mugica-Álvarez V (2018) Emission factors of atmospheric and climatic pollutants from crop residues burning. J Air Waste Manag Assoc 68:849–865

Shah M, Fawcett D, Sharma S, Tripathy S, Poinern GEJ (2015) Green synthesis of metallic nanoparticles via biological entities. Materials 8:7278–7308

Sinsinwar S, Sarkar MK, Suriya KR, Nithyanand P, Vadivel V (2018) Use of agricultural waste (coconut shell) for the synthesis of silver nanoparticles and evaluation of their antibacterial activity against selected human pathogens. Microb Pathog 124:30–37

Srikar SK, Giri DD, Pal DP, Mishra PK, Upadhyay SN (2016) Light induced green synthesis of silver nanoparticles using aqueous extract of *Prunus amygdalus*. Green Sustain Chem 6:26–33

Sriramulu M, Sumathi S (2018) Biosynthesis of palladium nanoparticles using *Saccharomyces cerevisiae* extract and its photocatalytic degradation behaviour. Adv Nat Sci Nanosci Nanotechnol 9:025018–025024

Thatikayala D, Jayarambabu N, Banothu V, Ballipalli CB, Park J, Rao KV (2019) Biogenic synthesis of silver nanoparticles mediated by *Theobroma cacao* extract: enhanced antibacterial and photocatalytic activities. J Mater Sci Mater Electron 30:17303–17313

Trivedi P, Khandelwa M, Srivastava P (2014) Statistically optimized synthesis of silver nanocubes from peel extracts of *Citrus limetta* and potential application in waste water treatment. J Microb Biochem Technol S4:1–7

United States Department of Agriculture (USDA) (2017) https://apps.fas.usda.gov/psdonline/circulars/citrus.pdf

Vairavel M, Devaraj E, Shanmugam R (2020) An eco-friendly synthesis of E*nterococcus* sp.–mediated gold nanoparticle induces cytotoxicity in human colorectal cancer cells. Environ Sci Pollut Res 27:8166–8175

Vanaja M, Rajeshkumar S, Paulkumar K, Gnanajobitha G, Malarkodi C, Annadurai G (2013) Kinetic study on green synthesis of silver nanoparticles using *Coleus aromaticus* leaf extract. Adv Appl Sci Res 4:50–55

Vasquez RD, Apostol JG, de Leon JD, Mariano JD, Mirhan CMC, Pangan SS, Reyes AGM, Zamora ET (2016) Polysaccharide-mediated green synthesis of silver nanoparticles from *Sargassum siliquosum* J.G. Agardh: assessment of toxicity and hepato protective activity. Open Nano 1:16–24

Verma A, Tyagi S, Verma A, Singh J, Joshi P (2017) Optimization of different reaction conditions for the bio-inspired synthesis of silver nanoparticles using aqueous extract of *Solanum nigrum* leaves. J Nanomater Mol Nanotechnol 6:2–6

Wen J, Salunke BK, Kim BS (2017) Biosynthesis of graphene-metal nanocomposites using plant extract and their biological activities. J ChemTechnol Biotechnol 92:1428–1435

Wilcoxon JP, Martin JE, Parsapour F, Wiedenman B, Kelley DF (1998) Photoluminescence from nano sized gold clusters. J Chem Phys 108:913–9143

Yang N, Li WH (2013) Mango peel extract mediated novel route for synthesis of silver nanoparticles and antibacterial application of silver nanoparticles loaded onto non-woven fabrics. Ind Crops Prod 48:81–88

Zamani A, Marjani AP, Mousavi Z (2019) Agricultural waste biomass-assisted nanostructures: synthesis and application. Green Process Synth 8:421–429